

Kelvin-Helmholtz Instability at the Magnetotail Boundary: MHD Simulation and Comparison with Geotail Observations

A. Otto, and D. H. Fairfield
Geophysical Institute, University of Alaska, Fairbanks

August 19, 1999

Short title:

Abstract. On March 24 1995 the Geotail spacecraft observed large fluctuations of the magnetic field and plasma properties in the Low Latitude Boundary Layer (LLBL) about $15 R_E$ tailward of the dusk meridian. Although the magnetospheric and the magnetosheath field were strongly northward, the B_z component showed strong short duration fluctuations in which B_z could even reach negative values. We have used two-dimensional magnetohydrodynamic simulations with magnetospheric and magnetosheath input parameters specifically chosen for this Geotail event to identify the processes which cause the observed boundary properties. It is shown that these fluctuations can be explained by the Kelvin-Helmholtz instability if the \mathbf{k} vector of the instability has a component along the magnetic field direction. The simulation results show many of the characteristic properties of the Geotail observations. In particular, the quasi-periodic strong fluctuations are well explained by satellite crossings through the Kelvin-Helmholtz vortices. It is illustrated how the interior structure of the Kelvin-Helmholtz vortices leads to the rapid fluctuations in the Geotail observations. Our results suggest an average Kelvin-Helmholtz wavelength of about $5 R_E$ with a vortex size of close to $2 R_E$ for an average repetition time of 2.5 minutes. The growth time for these waves implies a source region of about 10 to $16 R_E$ upstream from the location of the Geotail spacecraft (i.e., near the dusk meridian). The results also indicate a considerable mass transport of magnetosheath material into the magnetosphere by magnetic reconnection in the Kelvin-Helmholtz vortices.

1. Introduction

Processes at the boundary between the magnetosphere and the magnetosheath are of fundamental importance for the transport of plasma, momentum, and energy from the solar wind into the magnetosphere [Axford and Hines, 1961; Dungey, 1961]. Basic processes which facilitate this transport are magnetic reconnection, Kelvin-Helmholtz (KH) instabilities, and so-called pressure pulses. Whereas pressure pulses are driven by fluctuations in the solar wind, magnetic reconnection and KH instabilities are caused by the quasi-steady magnetic field and plasma configuration at the magnetopause, i.e., the boundary conditions imposed by the solar wind. The free energy for magnetic reconnection is provided by anti parallel components of the magnetic field across the magnetopause. Kelvin Helmholtz waves are caused by a gradient of the plasma velocity tangential to the magnetopause. All of the above processes have been subject to a variety of numerical studies [Miura and Pritchett, 1982; Lee and Fu, 1985; Wu, 1986; Liu and Hu, 1988; Scholer, 1988; Otto, 1990; Miura, 1992; Thomas and Winske, 1993; Wei and Lee, 1993; Fujimoto and Terasawa, 1995; La Belle-Hamer et al., 1995; Otto et al., 1995]. The most important effect of magnetic reconnection is the generation of open magnetic flux which is subsequently swept to the tail region. The KH mode is usually thought to be an important process for a quasi-viscous transfer of momentum and energy from the solar wind into the magnetosphere [Miura, 1984]. Since the KH mode is an ideal instability it is not expected to transport particles across the magnetopause or change the magnetic topology.

The motivation of this work has been a set of rather unusual plasma and magnetic field observations at the flank boundary of the magnetosphere as reported in a companion paper by Fairfield et al. [1999] to which we shall refer as KH2. On March 24, 1995 the Geotail spacecraft observed large fluctuations of the magnetic field and plasma properties at the duskside magnetospheric flank. At this time the spacecraft was in the LLBL about 15 R_E tailward of the dusk meridian. One of the most remarkable properties of the observations reported in KH2 is a very strongly fluctuating magnetic field with brief periods of negative B_z components although the interplanetary magnetic field (IMF) has remained strongly northward and largely parallel to the plasmasheet magnetic field during the entire event. The field fluctuations as well as the variation in the plasma properties show a clear quasi-periodic behavior with a period of 2 to 3 minutes.

While it is tempting to interpret strong magnetic field changes as being related to magnetic reconnection, the strongly northward magnetic field in the magnetosheath makes this interpretation difficult. At the satellite location the magnetosheath plasma velocity had a large negative x component and the magnetic field both on the magnetospheric and on the magnetosheath side are almost northward and perpendicular to the magnetosheath velocity (e.g., Figure 5b of KH2).

The onset condition for the Kelvin-Helmholtz instability is given by

$$[\mathbf{k} \cdot (\mathbf{V}_1 - \mathbf{V}_2)]^2 > \frac{n_1 + n_2}{4\pi m_0 n_1 n_2} [(\mathbf{k} \cdot \mathbf{B}_1)^2 + (\mathbf{k} \cdot \mathbf{B}_2)^2].$$

[e.g., Chandrasekhar, 1961] where \mathbf{V} denotes velocity, n number density, m_0 ion mass, \mathbf{B} magnetic field, the indices refer to the two regions across the shear flow layer.

With a \mathbf{k} vector of the KH mode mostly along the plasma flow and perpendicular to the magnetic field the magnetospheric boundary appears to be locally Kelvin-Helmholtz unstable. However, if the \mathbf{k} vector is exactly along the magnetosheath plasma velocity and exactly perpendicular to the magnetic field (in Figure 1 this corresponds to a situation with $\varphi = 0$), the field component in the plane of the Kelvin Helmholtz wave is 0. In this case the effect of the boundary wave is a quasi-periodic compression of the magnetic field but it does not alter the magnetic field direction. Thus this simple model of a KH wave is also unable to provide a satisfactory explanation for the strong magnetic field fluctuations.

A resolution of this problem becomes possible if one assumes a \mathbf{k} vector of the boundary wave

which is not exactly perpendicular to the magnetic field. In this case the magnetic field projected into the plane of the KH wave is nonzero but small and the twisting of this field component by KH vortices can strongly change the magnetic field in the KH plane and thereby alter the total magnetic field direction. There are two simple realizations of this configuration: (a) the \mathbf{k} vector is pointing in the $-x$ (i.e., the flow) direction and the magnetic field has a small x component, and (b) the field is northward and the \mathbf{k} vector has a small component out of the equatorial plane. Figure 1a and 1b illustrate these two configurations. The general case will be a mixture of the two cases with the additional complication that the magnetic fields on the magnetosheath and magnetospheric sides of the LLBL may not be exactly aligned.

A potential problem for an explanation of the observations in terms of a KH wave is the stabilization of the wave by the magnetic field. The twisting of a magnetic field by KH requires additional energy which lowers the growth rate or stabilizes the KH wave entirely.

This work attempts to clarify whether or not the KH instability can provide a satisfactory answer to the Geotail observations (KH2). It also provides a unique opportunity to compare actual in situ observations at the magnetospheric boundary with numerical simulations of a KH instability. This side by side comparison has the additional advantage that the normalization and initial conditions for the simulation can be chosen consistent with the real spacecraft observations thereby reducing ambiguities in the plasma parameters.

The actual computations are conducted using a two-dimensional MHD code with a relatively simple initial condition. The general situation to which our simulations apply is sketched in Figure 1c. The numerical method and initial conditions are introduced in the following section. Results of the numerical simulation are presented in section 3. Section 4 presents a summary and discussion of our results.

2. Numerical Method

The results in this study are obtained by using a two-dimensional MHD code. The basic equations for this method are in normalized form [e.g., *Otto*, 1990] and integrate the plasma mass density ρ , the plasma velocity \mathbf{v} , the plasma pressure p , and the magnetic field \mathbf{b} . All quantities are normalized to characteristic values for the system, i.e., length scales l to a typical length L_0 , density ρ to $\rho_0 = n_0 m_0$ with the number density n_0 and the ion mass m_0 , magnetic field \mathbf{b} to B_0 , velocity \mathbf{v} to the typical Alfvén velocity $v_A = B_0 / \sqrt{4\pi\rho_0}$, pressure to $P_0 = B_0^2 / (8\pi)$, and time t to a characteristic Alfvén transit time $\tau_A = L_0 / v_A$. The values for the normalization of the simulation units are summarized in Table 1. We will present most results in physical units such that explicit knowledge of the normalization is not needed unless otherwise mentioned.

Only length scales will be mostly presented in simulation units. The unit length of L_0 can be re-scaled if the same re-scaling is applied to time units. We use a simulation box of 40 units in x and a normalization of $L_0 = 600$ km corresponding to a wavelength of about $4 R_E$, $\tau_A = 5.7$ seconds, and a repetition time of 2 minutes for KH waves. The actual average repetition time appears closer to 2.5 minutes which can be taken into account by a re-scaling factor of 1.25 yielding a wavelength of $5 R_E$ and $\tau_A = 7.1$ seconds.

A large size of the simulation domain in y of approximately $12 R_E$ is used to minimize the influence of the boundary conditions on the evolution of the KH waves, for instance by reflection of waves from these boundaries.

The simulation employs a resistivity which is proportional to the magnitude of the current and is switched on for a current density above $1.1 J_0 = 23 \text{ nA m}^{-2}$ to avoid the evolution of too narrow and strong current sheets. We found that the precise choice of the resistivity has a negligible influence on

the dynamics.

The equations are solved with a finite differences Leapfrog scheme [Potter, 1973; Birn, 1980] which is of second-order accuracy in space and time. Basic properties of this code are described in Otto *et al.* [1995] and the method has been used for simulation of various systems and plasma processes [e.g., Otto, 1990; La Belle-Hamer *et al.*, 1995; Otto *et al.*, 1995; Chen *et al.*, 1997].

For comparison with the Geotail data the initial configuration for the simulation in the boundary coordinates of Figure 1a uses a magnetic field of $b_{x0}(x) = b_0(x) \sin \varphi$, $b_{y0}(x) = 0$, and $b_{z0}(x) = b_0(x) \cos \varphi$. The velocity is given by $v_{x0}(x) = v_0(x)$, $v_{y0}(x) = 0$, and $v_{z0}(x) = 0$. Initial density, pressure, velocity, and magnetic field magnitudes are:

$$\begin{aligned} \rho_0(x) &= \frac{1}{2}(\rho_{sh} + \rho_{sp}) + \frac{1}{2}(\rho_{sh} - \rho_{sp}) \tanh\left(\frac{y}{L_0}\right) \\ p_0(x) &= \frac{1}{2}(p_{sh} + p_{sp}) + \frac{1}{2}(p_{sh} - p_{sp}) \tanh\left(\frac{y}{L_0}\right) \\ v_0(x) &= -\frac{1}{2}v_{sh}(\tanh\left(\frac{y}{L_0}\right) + 1) \\ b_0(x) &= \frac{1}{2}(b_{sh} + b_{sp}) + \frac{1}{2}(b_{sh} - b_{sp}) \tanh\left(\frac{y}{L_0}\right) \end{aligned}$$

where the indices *sp* and *sh* correspond to the average values on the magnetospheric side and magnetosheath side of the magnetopause boundary. The initial condition presents a one-dimensional steady state where the magnetic field magnitudes $b_{sh} = 24$ nT and $b_{sp} = 16$ nT are chosen to agree approximately with the measured fields (KH2). The difference in thermal pressure is determined by total pressure balance. The magnetosheath pressure is determined using a number density of 19.2 cm^{-3} and a temperature of 50 eV. Assuming magnetospheric density of 2.8 cm^{-3} yields a temperature of 650 eV on this side. For the presented results the chosen values for the initial magnetic field and plasma properties are summarized in Table 2. For an evaluation of the properties of the KH mode for different parameters, we have carried out additional simulation runs with different magnetosheath velocities and angles φ as given in Table 3. We also included one case (number 11) representing the configuration in Figure 1b. For this case the velocity in the simulation plane is $v_{x0}(x) = v_0(x) \cos \varphi$, $v_{y0}(x) = 0$, and $v_{z0}(x) = v_0(x) \sin \varphi$ and the magnetic field is determined by $b_{x0}(x) = -b_0(x) \sin \varphi$, $b_{y0}(x) = 0$, and $b_{z0}(x) = b_0(x) \cos \varphi$.

The two-dimensional simulations are performed in the plane determined by the direction normal to the magnetospheric boundary y and the \mathbf{k} vector of the instability. For the configuration illustrated in Figure 1a this corresponds to a boundary normal system with x generally pointing sunward along the magnetospheric boundary, y being normal to the average magnetopause, and z being northward along the tail boundary. For the configuration depicted in Figure 1b the simulation coordinates are rotated in the x, z plane by an angle of φ compared to the boundary normal system of Figure 1a. Thus determination of the boundary normal b_z component in the configuration of Figure 1b requires the corresponding transformation.

The initial state of the simulation uses a Galilei transformation for the velocity such that the simulation frame is moving with half the magnetosheath velocity. In this manner the KH vortex is moving slower in the simulation frame, with the advantage, that the time step limit for the integration of the MHD equation is larger than in a frame which is at rest with the magnetosphere. In other words the simulation frame illustrated in the sketch in Figure 1c is sliding with half the magnetosheath plasma velocity tailward.

Boundary conditions for the simulations are periodic along the x direction and boundary conditions in y are open to inflow and outflow of plasma. The simulations typically use 303 by 403 grid points (in x and y) which are uniformly spaced in x with a resolution of about 80 km and non-uniformly spaced

in y with a maximum resolution of about 60 km at $y = 0$ at the location of the magnetopause where the KH wave develops. We have carried out simulations with twice the number of grid points with virtually no difference of the results on the considered time scales.

The initial perturbation for the KH mode is not an exact eigenmode but an incompressible initial perturbation in the plasma velocity consistent with the KH wave. The same type of perturbation is used in Chen et al. [1997]. The amplitude of the perturbation in the y direction (normal to the original boundary) is about 1 km s^{-1} . Note that although we don't know the precise spectrum of the initial perturbations, typical values for the perpendicular motion at the magnetopause are of the order of about 10 km s^{-1} such that the chosen initial perturbation appears reasonable for a single mode. Also, the time scale on which the KH becomes nonlinear does not depend strongly on the choice of the initial perturbation because of the exponential growth of the linear mode.

It is worth revisiting the main assumptions which went into the simulation set up. If the observed Geotail spacecraft signatures are caused by KH waves, these must have originated somewhere upstream of the spacecraft. The perturbations are probably such that not a single wave but an entire spectrum of waves is generated and different growth of different modes and changes this spectrum as the waves move along the magnetospheric boundary [Miura, 1999a, 1999b]. Clearly the simulation cannot consider the shape of the magnetospheric boundary and the change of plasma and field parameters. To obtain basic results only a single mode is investigated in each simulation run for most of the runs which we have performed. Finally, the simulations presented here are all two-dimensional. Modes with different orientations of the \mathbf{k} vector may originate from different latitudes. A three-dimensional model is needed if two or more modes with different \mathbf{k} orientation are dominant for a particular spacecraft observation. Similarly a potential stabilization of the KH modes by line-tying of the magnetospheric magnetic field is a three-dimensional effect and not considered in the present simulation.

2. Results

Evolution of the KH wave

The evolution of the KH wave is illustrated in the plots in Figure 2. We will refer to the case in Figure 2 as the reference case (case 3 in Table 3) which uses a magnetosheath velocity of 315 km s^{-1} and an angle of $\varphi = 25^\circ$ for the magnetic field orientation yielding a positive B_x component of 6 to 10 nT on the two sides of the boundary. The arrows in these plots illustrate the orientation and magnitude of the plasma velocity in the simulation plane and the lines are magnetic field lines projected into this plane. All plots show a region from $x = -30$ to $x = 10$ (using the periodicity in x) for a better visualization of the KH vortex evolution.

The asterisks in the plots represent plasma elements which were initially uniformly spaced along the line $y = 0$. Their location is computed by integrating the path of these elements using the plasma velocity. Considering $y = 0$ to be the original boundary the asterisks are indicators for the change of this boundary. The region to the left (negative y) will be addressed as the magnetospheric region and the region to the right as the magnetosheath region based on the chosen plasma and field properties. The star in each plot refers to a location where plasma and field properties have been recorded for an illustration of plasma and field signatures.

For the chosen initial perturbation it takes about 4 minutes for the wave to develop to a size which shows up as a clear boundary wave. The first plot in Figure 2 shows the magnetic field and plasma flow in our simulation plane at $t = 262 \text{ s}$. The KH vortex is clearly visible, however, at this time it has not produced a curl in the magnetic field in this plane. The next plot (top right) shows the system at $t = 358 \text{ s}$. The KH mode is now twisting the magnetic field and there are regions in the simulation domain with a field direction opposite to the original orientation in the x, y plane. This implies that

the KH instability already leads to changes in the magnetic field orientation. The twist of the magnetic field intensifies as illustrated by the plot for $t = 424$ s. Note that the separation of the projected field lines is a measure of the magnetic field strength in this plane indicating that the KH vortex leads in addition to a filamentary structure with stronger and weaker magnetic fields in the vortex. During the late evolution the vortex becomes distorted ($t = 490$ s), with substructures and smaller vortices present within the main structure.

The original boundary identified by the asterisks remains quite well defined up to about 6 minutes into the simulation. However, the the plasma elements from this boundary are swept into the vortex even at early times. The last two plots show a strong accumulation of these plasma elements in the center of the vortex with many of these elements sitting now on separate magnetic islands. We will address this peculiar behavior later while discussing the physical mechanisms and magnetic reconnection.

Growth and stabilization

The sequence of plots in Figure 2 demonstrates that the KH vortex is not at rest in the simulation frame. For a very thin boundary we expect the KH mode to propagate in a frame moving with a velocity of

$$V_{kh} = V_{sh} \frac{\rho_{sh}}{\rho_{sh} + \rho_{sp}}$$

(Chandrasekhar, 1961). For the given parameters this implies a velocity of 275 km s^{-1} relative to the magnetosphere (which is assumed at rest). For a boundary with a very small density gradient (approximately constant density) KH waves should move with half the magnetosheath velocity, i.e. 157 km s^{-1} . Using the results from Figure 2 we obtain a velocity of about 220 km s^{-1} which we attribute to the presence of a finite density gradient at the initial boundary.

A main concern for KH modes with a magnetic field component along the \mathbf{k} vector is the stabilization of these modes by the magnetic field. Figure 3 shows the growth of the KH measured by the magnitude of the velocity perturbation for different simulation cases varying the angle φ (top) and varying the sheath velocity (bottom). The plot in (a) shows a slight decrease in the growth of the KH wave for increasing φ , i.e., for increasing magnetic field tangential to the tailward plasma flow. Here the magnetosheath velocity is fixed to 315 km s^{-1} . The plot in (b) demonstrates a decrease of the growth with decreasing magnetosheath velocity for a fixed angle $\varphi = 25^\circ$. The solid line in both plots corresponds to our reference case.

This behavior is expected. For a KH mode in an ideal incompressible plasma with a discontinuous (arbitrarily thin) velocity shear layer the growth rate q of the wave is given by

$$q = [\alpha_1 \alpha_2 [(\mathbf{V}_1 - \mathbf{V}_2) \cdot \mathbf{k}]^2 - \alpha_1 (\mathbf{V}_{A1} \cdot \mathbf{k})^2 - \alpha_2 (\mathbf{V}_{A2} \cdot \mathbf{k})^2]^{\frac{1}{2}}$$

(Chandrasekhar, 1961) where the indices refer to the two sides of the shear flow layer, $\alpha_i = \rho_i / (\rho_1 + \rho_2)$, and $\mathbf{V}_{Ai} = \mathbf{B}_i / \sqrt{4\pi\rho_i}$. For our geometry with the angle φ as illustrated in Figure 1a this expression yields

$$q = k \sqrt{\alpha_{sh} \alpha_{sp} V_{sh}^2 \cos^2 \varphi - (\alpha_{sh} V_{Ash}^2 + \alpha_{sp} V_{Asp}^2) \sin^2 \varphi}.$$

Note that V_{sh} needs to be replaced by $V_{sh} \cos \varphi$ for configuration (b).

An increase of φ leads to an increase of the magnetic field tangential to the \mathbf{k} vector and thus to a stabilization of the mode. An increase of the magnetosheath velocity yields an increase in the growth rate.

For the relevant parameters the plots in Figure 4 show the dependence of the growth rate q on the angle φ for the fixed magnetosheath velocity of 315 km s^{-1} (upper plot) for the configuration of

Figure 1a (solid line) and Figure 1b (dashed line). The bottom plot illustrates the growth rate as a function of the magnetosheath velocity for the angles $\varphi = 15^\circ$ and $\varphi = 25^\circ$. The scale of the growth rate assumes a wavelength of 24000 km, i.e., the wavelength chosen for our reference case. The black squares indicate the growth rates we obtained from the simulation results of Figure 3. Overall the simulation results are consistent but somewhat smaller than implied by the dispersion relation. This is expected because of the finite width of the shear layer and because of plasma compressibility which are not considered in the dispersion relation [Miura and Pritchett, 1982].

The plots demonstrate that although the growth rate depends on the angle φ this effect is only significant for angles larger than 30° . In fact the growth rate for $\varphi = 25^\circ$ is only reduced by 16 % when compared to $\varphi = 0$. The lower plot in Figure 4 illustrates that the growth rate for a fixed angle $\varphi = 25^\circ$ does not change significantly unless the magnetosheath velocity drops to values of 250 km s^{-1} and lower. The dispersion relation implies a growth time of $\tau_g = 45 \text{ s}$ compared to $\tau_g = 55 \text{ s}$ from the simulation for our reference case.

With respect to the stabilization of the KH mode by the magnetic field component along the \mathbf{k} vector, neither moderate variations of B_x nor moderate variations of the magnetosheath velocity have a strong influence on the growth of the KH wave. Since all modes with small variations of B_x grow with about the same rate, the initial perturbation spectrum should have a significant influence on the spectrum of KH modes which are observed after 4 to 5 growth times. With a growth time of about 60 s and a phase velocity of $200 \text{ to } 250 \text{ km s}^{-1}$ a KH vortex has moved about 8 to $12.5 R_E$. For an average repetition time of 2.5 minutes (KH2) a re-scaling with a factor of 1.25 yields a growth time of 75 s and a source location at 10 to $16 R_E$ upstream of the satellite.

Signatures

One of the most surprising results reported in the KH2 observations is the strong variation of the magnetic field despite the fact that the average field is strongly northward on the magnetospheric and on the magnetosheath side at the satellite location. The sequence of plots in Figure 2 already indicates a twisting of the magnetic field by the evolving KH vortex. Figure 5 represents what a virtual spacecraft would observe moving through the simulation box at a location just outside the original magnetosphere at $y=1.5$ ($Y=900 \text{ km}$). We emphasize that it is not what a real spacecraft would see because the virtual spacecraft sees the periodic signature of an aging Kh wave. Different age KH vortices in terms of growth times can be seen by a real spacecraft for instance if the wave length changes, for different amplitudes of the upstream perturbation, or for changing distances from the upstream source.

The recording location at the times of the four plots in Figure 2 are indicated by stars in this figure. This location moves with a velocity of 157 km s^{-1} into the positive x direction such that it is in the plasma rest frame of the magnetospheric side of the simulation box. The encircled numbers at the bottom plot of Figure 5 indicate times for which plots are shown in Figure 2.

In particular the shaded high density regions are good markers for distinct quasi-periodic intervals of similar sheath-like plasma and field properties. Such periods of higher density are associated with larger magnetic field magnitude (the magnetosheath field is larger than the magnetospheric magnetic field) particularly of the z component, with low plasma temperature, and with relatively steady plasma velocity. Intervals with lower density are associated with lower average field strength, with higher temperature, and overall stronger fluctuations. This is particularly well visible in the z component of the magnetic field which shows very strong fluctuations with a pronounced minimum just prior to the high density sheath-like regions. We will refer to this transition as the outbound pass. It is also characterized by extrema in the B_x and B_y components of opposite polarity.

A comparison with Figure 2 demonstrates that the probe is just prior to an outbound pass in the first plot of Figure 2, it just left the core of the vortex in the second plot, it is about to make an

inbound pass in the third plot, and it is in an outbound pass in the last plot.

The quasi-periodic intervals show a number of common plasma and magnetic field properties. Thus instead of recording data as a function of time in one location Figure 6 shows two cuts at constant y and for $t = 358$ s (corresponding to the second plot in Figure 2) through the 2D system. For an easier comparison and identification of individual characteristic features we have shown the dataset for two periods. The plots use a similar data format as Figure 5 but use x instead of time for the axis. For the chosen parameters and vortex velocities a length unit translates into approximately 3 s. The arrows in Figure 6 indicate the actual dimension (in x) of the simulation box in the corresponding Figure 7.

The upper plot in Figure 6 is a cut at $y = 2$ (1200 km), i.e., close to the path of the probe, and the lower plot uses a cut at $y = -3$ (-1800 km). Marked by different shading in the plot are a number of different regions with characteristic properties. The light shading indicates a region with high sheath-like density, the darker shading indicates a region of high temperature and low density, and the vertical line indicates an additional boundary.

Both cuts show similar properties with some slightly more pronounced in the bottom plot such that we labelled distinct intervals using a lettering from (a) to (e) in this plot. The labelling is similar to the one chosen in KH2 (Figure 7b) with the exception that region (a) of KH2 is split into (e) and (a) in Figure 6.

Region (a) represents the core of the KH vortex and is characterized by strong fluctuations virtually in all plasma and field properties. The region can show high density spikes somewhat resembling sheath-like properties (higher B_z , etc.). Often visible in this region are reversals of V_y which can be accompanied by changes in V_x .

Region (b) shows fairly steady plasma and field properties, with magnetospheric-like high temperatures and relatively low densities. Characteristic for this region is also the a fairly steady decrease of the V_y component.

Region (c) characterizes the outbound transition just prior to the high density intervals. Typical for region (c) are the decrease of temperature and increase of density, a high total magnetic field magnitude, a pronounced minimum in B_z , and extrema in the B_x and B_y components. The local maxima and minima in B_x and B_y are often accompanied by a minimum of B_z prior to the sheath-like intervals with larger and steady B_z . The outbound pass is often fairly easy to identify in the Geotail data (KH2, Figure 7b).

Region (d) shows the already mentioned high number density and low temperature, large B_z , and fairly steady plasma and field properties, i.e., magnetosheath-like properties.

Finally, the region (e) marks the inbound pass into a region of generally lower number density and intermediate or high temperature. It shows a less pronounced minimum in B_z , and frequently an extremum in B_y (sometimes in B_x depending on the normal direction of this boundary).

A comparison of the plots of Figure 6 also demonstrates that in general the length of high density intervals decreases with distance from the magnetosheath.

Physical mechanisms

To reconcile the characteristic regions with the physics of the KH wave, Figure 7 shows a plot of the magnetic field with a gray scale plot of B_z (top) and of a gray scale plot of the number density combined with magnetic field vectors (bottom). The two vertical lines indicate the location at which the cuts for Figure 6 are chosen.

The magnetic field plot illustrates a strong depletion of B_z outside the vortex in the vicinity of the original boundary. For a simple identification we will address this region as the spine of the KH wave. Obviously the spine region is also characterized by large B_x and B_y components and it extends partially into the vortex. Any outbound pass has to cross this spine region and would show typical extrema in

B_x and B_y with different polarity. The KH vortex motion leads to a twisting of the magnetic field which accounts for the strong variations of the field in the vortex. It is also illustrated that the plasma motion sweeps high density magnetosheath material into the vortex such that individual spikes of high number density are present in the vortex region. In addition, the second plot of Figure 2 demonstrates a steady decrease of the V_y in the wake of the vortex in the low density region.

For the large magnetic field magnitude along the spine and the depletion of the B_z component in the same region our simulation results suggest the following explanation. During the early evolution (from about 200 s to 360 s, or 3 to 6 τ_g) the KH vortex region develops a strong depletion of the static total pressure resulting from the centrifugal forces of the vortex motion. This is visible in the total pressure plot in Figure 5. Plasma motion along those field lines which are swept into the vortex fills the vortex with plasma from the region of the original boundary. This is illustrated by the distribution of asterisks in Figure 2 and their accumulation in the core of the KH vortex. Originally the corresponding plasma elements were uniformly spaced along the boundary. The divergent motion of plasma along the spine into the vortex is compensated by a convergent motion (perpendicular to the magnetic field in the simulation plane) toward the spine region. This motion leads to an accumulation of B_x and B_y flux in the vicinity of the original boundary along the spine region.

The divergent motion and the different compressibility of plasma and field lead to the depletion of the B_z component. One can also argue that the large field along the spine region implies a minimum of B_z in the spine because of approximate total pressure balance across this boundary. Note that this evolution eventually leads to a stabilization of the vortex motion because the increasing magnetic field along the spine requires a larger energy in order to twist the magnetic field. It is expected and indicated by our results that the stabilization occurs when the magnetic field energy density (based on the B_x and B_y components) approaches the energy density of the shear velocity in the boundary region. This leads locally to an approximate equipartition between kinetic energy of the bulk flow and the magnetic energy which may be relevant for astrophysical systems [Birk *et al.*, 1999].

Magnetospheric signatures and magnetic reconnection

Figure 8 shows two cuts further on the magnetospheric side and at later times than Figure 6. These cuts illustrate that intervals of low density magnetospheric plasma are increasing in length with distance from the magnetosheath. However, there are still brief encounters of high density sheath-like plasma. This raises the question whether these encounters are actually outbound passes. A comparison of the shaded high density region (centered at $x = -25$) upper plot of Figure 8 with the two-dimensional density and field plot of Figure 9 (see also the third plot of Figure 2) indicates that this region is indeed a magnetosheath encounter. However, of the following 2 smaller density spikes in Figure 8 (centered at $x = -15$ and $x = -12$), the first is in the core of the vortex in Figure 9, i.e., in a region which is entirely embedded in the magnetospheric region while the second is still magnetically connected to the sheath (the lower part of the vortex arm in Figure 9).

Figure 9 already illustrates a small region in the core of the vortex which is filled with plasma elements from the original boundary and entirely detached from the sheath region. Note that the vortex contains two more plasma blobs which appear as being squeezed from their connection to the magnetosheath. This is indeed happening as illustrated by the last plot of Figure 2. This plot illustrates a large region within which two larger magnetic islands contain actually most of the plasma elements from the original boundary. This entire region is detached from the magnetosheath. The bottom plot of Figure 8 shows plasma and field data in a cut at $y = -10$ (-6000km) at the time of the last plot of Figure 2. The plot in Figure 8 illustrates a clear density spike showing all of the properties characteristic for the encounter of magnetosheath-like plasma and the corresponding transition regions. However, this region is totally detached from the magnetosheath.

As a last example Figure 10 illustrates boundary wave signatures for the case (7) with $\varphi = 15^\circ$ (with the same sheath velocity of 315 km s^{-1}) at $y = -8$ (-4800 km) and $t = 463$. Figure 11 shows the corresponding two-dimensional plots of the plasma velocity (V_x and V_y as arrows and V_z in gray scale, top figure) and the number density (gray scale, bottom), and Figure 12 presents the magnetic field (B_x and B_y as arrows and B_z in gray scale, top figure) and the current density (J_x and J_y as arrows and J_z in gray scale, bottom figure). The current density is measured in 10^{-9} A m^{-2} . The vertical line in Figure 11 illustrates the location for the cut in Figure 10 and demonstrates that the first brief density spike centered at $x = -27$ (Figure 10) represents a grazing encounter of the magnetosheath. This brief encounter shows many characteristic features but does not have a pronounced increase of B_z in the high density region.

The second density increase in Figure 10 centered at $x = -12$ shows all typical properties except for the depletion of B_z in region (c). This encounter is of high density plasma which is no longer magnetically connected to the sheath. The density plot in Figure 11 illustrates that the high density plasma can cover a large region which is not magnetically connected to the magnetosheath.

The plots in Figure 11 also illustrate that the vortex for this case is larger and appears more distorted than for the reference case. The magnetic field (lines in the top plots of Figure 11 and 12) exhibits various smaller and larger magnetic islands. As in the reference case most of the plasma of the initial boundary is now contained in individual small islands. The velocity has formed various smaller vortex motions. Well visible in this case is also the spine region with a large magnetic field component in the KH plane along the boundary between sheath and magnetospheric plasma, and the depletion of B_z in this region.

Similar to the reference case, the magnetic field and the density in the vortex appear to being pinched from the rest of the magnetosheath plasma and field. This is in fact caused by magnetic reconnection. The top plot of Figure 12 shows a magnetic X line at $x = -23$, $y = -10$. It is instructive to compare this with the current density which is enhanced at the location of the X line (Figure 12, bottom). In fact the vortex is filled with many current filaments with current directed in the positive and in the negative z direction. The solid line in the current density plot is chosen by the location of the plasma elements from the initial boundary, such that this line represents in the best accountable way this initial boundary. Note that despite the current dependent resistivity which switches on at $J_{crit} = 23 \text{ nA m}^{-2}$ the current density is twice as large. We have tried larger values of J_{crit} but the actual current densities in the vortex seem to surpass any value which is possible within the numerical limitations.

There are two mechanisms participating in the formation of the current filaments. First, the vortex motion twists the magnetic field. This generates multiple layers of magnetic flux with alternating magnetic field orientation and thus requires the presence of alternating currents. Second, the mechanism by which the spine is forming leads to a layer of large magnetic field along the spine region with a depletion of B_z . This also requires the presence of the corresponding currents which are visible in Figure 12. Since the magnetic field of the spine extends into the vortex, some of the current (bounding the spine) exist in the vortex region. Both mechanisms lead to the formation of the multiple current filaments visible in Figure 12.

We found for all cases that the pinching is larger on the magnetospheric side. Reconnection first snaps off smaller flux tubes in the high density filaments of the vortex, as seen for instance in the third plot in Figure 2. After about 6 to 7 minutes magnetic reconnection intensifies in the outermost vortex arm on the magnetospheric side and pinches off most of the plasma inside the vortex. Reconnection continues in various locations changing the interior magnetic topology of the vortex. In all cases the reconnection rate is high and close to the *Petschek* [1964] rate. The reason for the onset of reconnection first in the high density region is possibly caused by the initially larger field (also B_x component) on

the magnetosheath side and the higher inertia which drags this field into the vortex arms. A test run with the larger field on the magnetospheric side yielded reconnection first on the magnetosheath side.

In two dimensions the final fate of the captured high density filament must be reconnection with the magnetosheath. This is enforced by the magnetic configuration. The magnetic field of the island in Figure 12 (top) is parallel to the field on the magnetospheric side and anti-parallel to the field on the sheath side. The current density plot also shows the presence of a large negative current (dark) between the island and the magnetosheath boundary. Thus for topological reasons the filament should eventually merge back into the magnetosheath which indeed takes place at rather late times (after about 10 growth times or 10 minutes). However, this topological constraint does not apply in three dimensions where an interchange motion may move the flux tube further into the magnetosphere.

Symmetry and other transformations

The observations reported in KH2 demonstrate the frequent occurrence of a positive B_x and a negative B_y component in the transition region (c) (Figure 6) from low to high density plasma. However, in some cases the opposite polarity is observed in KH2. Since the magnetic field along the spine region (c) (Figure 6 and 7) is amplified from its original (background) value, the orientation and thus the polarity of the spine magnetic field is determined by the initial (boundary) B_x component.

In fact also the symmetry of the MHD equations imply a inverse sign for B_x , B_y , and V_z if the initial (or boundary value of) B_x has the opposite sign. Thus the corresponding observations with opposite polarity ($B_x < 0$ and $B_y > 0$) during an outbound pass on the duskside imply a different orientation of B_x , i.e., the magnetic field component parallel to the \mathbf{k} vector of the KH wave. This signature either implies small negative initial/boundary values of B_x or a small positive z component of the \mathbf{k} vector such that the initial magnetic field projected onto the \mathbf{k} vector has a small negative x component as illustrated in Figure 1b.

An initial B_x with different signs on the magnetospheric and magnetosheath sides implies the evolution of a bipolar rather than the monopolar signature for B_x (and for B_y) in the spine region (c). The same symmetry arguments apply to the polarity of B_x , B_y , and V_z in other regions of the boundary wave.

The sign of the B_x and B_y perturbations also depends on a duskside or dawnside flank location. On the dawnside flank these magnetic field signatures should show the same polarity (i.e., either $B_x < 0$, $B_y < 0$ or $B_x > 0$, $B_y > 0$) during outbound transitions which is indeed seen in the corresponding dawnside observations [Chen and Kivelson, 1993; Chen et al., 1993].

We note that a tilt of the \mathbf{k} vector out of the equatorial plane has also other implications. The characteristics of the spine region as discussed apply to the plane in which the KH wave is operating. For instance, if the \mathbf{k} vector has a positive z component, a comparison of simulation with observations requires that magnetic field and velocity signatures be determined in GSM coordinates. This implies a rotation of the simulation results by the angle φ (Figure 1b). This rotation modifies the x and z components of the the magnetic field and the velocity. As an example Figure 13 illustrates the magnetic field for a case where the \mathbf{k} vector is tilted by 25° as illustrated in Figure 1b. The gray scale plot (top) shows the B_x component in the simulation plane and the bottom plot illustrates in gray scale the B_{zmsp} component in the magnetospheric frame. It is obvious that the minimum of B_{zmsp} is now shifted to a different location. The transformation implies that large negative B_x components in the simulation plane lowers the B_{zmsp} component. This yields a minimum of B_{zmsp} in the vortex.

This example also illustrates a case in which B_{zmsp} is actually negative. We remark that negative values are also sometimes obtained in the other simulation cases, however, only in very narrow regions and intermittently. Without illustration we remark that B_x signatures are less effected by the transformation. However, the V_{zmsp} component is typically larger in the configuration of Figure 1b.

Finally, transformations resulting from the shape of the magnetopause and transformations resulting from the flaring of the magnetosphere modify the signatures from those reported here. However, if the corresponding angles are small, these are usually minor modifications leaving the typical features intact.

Further analysis

We have carried out a variance analysis on the data obtained from the simulation. Without illustration it is worth noting that the minimum variance of the magnetic field in Figure 6 for the cut at $y = 2$ (top) gives good normals to the actual current layers. For instance, the inbound normal at $x = -18$ (corresponding to the region (e) in the bottom plot of Figure 6) for the cut at $y = 2$ is tilted by 97.5° and the outbound normal at $x = 4$ (corresponding region (c)) is tilted by 33.5° (measured from the y direction toward positive x). The plots of Figure 7 illustrates the location and tilt of these boundaries. A good agreement is somewhat expected because the current layers move very fast across a point of observation such that their structure doesn't change significantly during the brief encounter.

We also note that a determination of a normal direction by using 2 points in space yields good results if the 2 points have a sufficient separation along the normal direction. If the satellite locations are on different sides of the boundary the crossproduct of the magnetic field should define the normal direction if the boundary is one-dimensional and time independent on the scales defined by the satellite separation. However, if the two points are very close and/or separated along a direction mostly perpendicular to the actual normal one expects considerable errors because these points are not anymore on opposite sides of the boundary at any time or will be so only for extremely brief periods of time. As a result the magnetic fields at the two locations are fairly aligned and small variations of the magnetic fields can cause large errors in the attempt to identify a normal by the crossproduct of the magnetic field vectors. This may be relevant in view of some of the results by *Chen and Kivelson* [1993], where ISEE 1 and 2 were separated primarily along y . In such a configuration it can be difficult to identify the inbound normals. Figures 2 and 7 illustrate that the inbound passes should show large variations of the boundary normal including large deflections which is in excellent agreement with the results in KH2.

In a last data analysis we minimized the square of the convection electric field in an attempt to find a de Hoffmann-Teller frame [Sonnerup *et al.*, 1990]. We indeed found an excellent frame with a pronounced minimum. A plot of the actual versus the de Hoffmann-Teller electric field yields correlation coefficients of 0.99. The transformation velocity is in the range of 210 km s^{-1} to 250 km s^{-1} with larger velocities closer to the magnetosheath. The velocity variation in the vortex is small compared to the vortex speed and mostly field-aligned. Thus a minimization of the electric field magnitude yields a good approximation to the actual vortex speed along the magnetosphere.

3. Summary and Discussion

This work studies the evolution of KH wave along the magnetospheric boundary in the presence of a small magnetic field component along the \mathbf{k} vector of the wave. It has been motivated by observations reported in our companion paper KH2 which showed unexpectedly large magnetic perturbations including deep minima of the B_z component in the LLBL even though the IMF and the magnetosheath field are strongly northward.

It is shown that the presence of a small magnetic field component along the \mathbf{k} vector of the boundary wave leads indeed to large magnetic perturbations of all three field components. The vortex motion generates a strongly twisted field. In addition plasma flow along magnetic field lines into the vortex generates a spine region (see physical mechanisms) which connects neighboring KH vortices along the magnetospheric boundary. In the x, y plane the magnetic field along the spine is

strongly amplified while the perpendicular B_z component is depleted. Outbound passes of a satellite generally occur through the spine showing typically extrema of opposite polarity in the B_x and B_y components and a pronounced depletion of the B_z component. Inbound passes usually occur into the KH vortex encountering an extremum of the B_y component often also accompanied by a smaller depletion of B_z and, depending on the location, an extremum in B_x . Within the vortex, density spikes with magnetosheath-like properties can be present and strongly fluctuating magnetic fields are typical. Trailing the main vortex is a region of more magnetospheric character typically showing a steady decrease of the V_y component. The sign of the B_x , B_y , and V_z signatures depends on the sign of the initial B_x (and the orientation of the \mathbf{k} vector). A component of the KH wave vector out of the equatorial plane has some impact on the B_z signatures.

Encounters of sheath-like plasma should on average be shorter with distance from the magnetosheath. Frequently filaments encountered further on the magnetospheric side may indeed be detached or partially detached from the magnetosheath even though they might exhibit all typical sheath properties (within the limitations of the fluid model). Thus it may observationally be difficult to distinguish true sheath encounters from detached plasma blobs of sheath origin. However, electron distribution functions may identify such regions [Fujimoto *et al.*, 1998a].

The signatures inferred from the simulation agree well with many of the signatures of the March 24 1995 Geotail event (KH2). They also appear to agree well with signatures from earlier work [Chen and Kivelson, 1993; Chen *et al.*, 1993] although we do not have an explanation for a discrepancy regarding the normal direction and the interpreted wave form in this work. However, it is noted that the boundary normals in this work are determined differently from KH2. The determination of a boundary normal by the crossproduct of the magnetic field at two closely spaced satellite locations requires that the normal has a considerable component along the satellite separation.

For our reference case the KH vortex moves with a speed of 220 km s^{-1} . Thus a wavelength of $4 R_E$ implies a repetition time of vortex structures of about 2 minutes. With an initial perturbation amplitude of 1 % the wave requires about 5 growth times $\tau_g = 55s$ (for a wavelength of $4 R_E$) to reach a nonlinear amplitude with many of the reported properties. A repetition time of 2.5 minutes (KH2) corresponds to a wavelength of $5 R_E$, a growth time of 70 seconds, and a source region at about 10 to 16 R_E upstream of the spacecraft. Repetition time and the distance to the upstream source scale linearly with the wave length. The observation of longer periods with quasi-periodic boundary signature further downtail [Fairfield *et al.*, 1996] is expected from the above arguments.

Our results indicate that reconnection in the KH vortices should be a common occurrence. The sketch in Figure 14 summarizes the basic aspects. First the vortex motion of the KH wave generates a strongly twisted magnetic field (labelled B). Within the vortex the layers of different magnetic field orientation must be separated by current layers (dashed). Note that we expect a strongly enhanced growth of tearing modes in such alternating current layers [Otto and Birk, 1992; Yan *et al.*, 1994]. During the evolution the current density increases to very large values giving rise to magnetic reconnection at varying locations in the KH vortex. Reconnection in the high density arm of the main vortex finally detaches a large scale high density filament from the the magnetosheath region. In three dimensions interchange motion might be able to move the detached density blobs further into the magnetosphere. Clearly this scenario is very much based on the two-dimensional approximation and may change in a more complex three-dimensional model. However, the observation of high density and low temperature filaments deep in the magnetosphere [Fujimoto *et al.*, 1996, 1998b] and the dependence of the plasma sheet density on solar wind density [Borovsky *et al.*, 1998] can be explained by plasma entry through reconnection in KH waves.

Usually the KH mode is thought to be a source for viscous coupling [Axford and Hines, 1961; Miura, 1984]. In the following we estimate the actual plasma transport for reconnection in KH vortices.

A plasma filament detaches after about 7 to 8 growth times or 450 seconds (corresponding to a traveling distance of about $15 R_E$ along the magnetospheric boundary). The detached filament has a size of roughly $1 R_E^2$ corresponding to a width of $1/4 R_E$ when averaged over the length ($4 R_E$) of the wave. With a sheath velocity of 300 km s^{-1} this yields an average mass diffusion velocity of 5 km s^{-1} perpendicular to the magnetopause boundary. Three-dimensional effects may reduce or enhance this value. Note that this estimate is rather crude considering only a single wavelength.

For sufficiently thin boundaries in the KH vortex, fast anomalous diffusion is observed in hybrid and full particle simulation [Fujimoto and Terasawa, 1994; 1995; Thomas and Winske, 1993]. The filamentary field structure and multiple reconnection sites may further enhance the diffusive transport. However, reconnection can generate a large scale mass transport even without anomalous diffusion (with the possible exception of the diffusion region at X lines).

Our results of reconnection in a KH vortex are distinct from so-called vortex induced reconnection [e.g., Liu and Hu, 1988; Pu et al., 1990]. This earlier work refers to the interaction of the KH mode and the tearing mode on the same scale. Chen et al. [1997] have shown that these instabilities occur mutually exclusive in two dimensions if they have the same wavelength. In our case reconnection occurs on a much finer scale than the primary KH mode. In fact our initial configuration is not tearing unstable because the initial magnetic field on the two sides of the boundary is parallel.

The properties described in this work depend on the presence of a B_x component in the initial configuration. In the absence of this component, signatures change drastically and magnetic reconnection is not possible. Even for relatively small values of B_x the basic properties remain present, however, it will take a longer time to develop the spine feature and to accumulate sufficient magnetic flux for magnetic reconnection. Too large values of B_x will stabilize the mode or prohibit a sufficient rotation of the vortex flow. In the range of $\varphi = 10^\circ$ to 30° corresponding to $B_x = 4$ to 12 nT (for the chosen flow and plasma properties) the changes are more gradual and the overall evolution and temporal scales are similar.

Finally, our model is subject to several limitations. The problem under consideration is actually a boundary value problem rather than an initial value problem. We consider in the simulation only the evolution of a single mode rather than a spectrum with various \mathbf{k} vectors, and the present approach is only two-dimensional. These limitations should be kept in mind for the interpretation of the reconnection process. The reconnected filaments actually represent magnetic flux tubes for which the magnetic connection is not defined without the larger scale 3D structure. Our approach allows to focus on more detail and to clarify important two-dimensional physics. The comparison with the observations reported in KH2 suggests that the present model captures much of the relevant physics. For very thin current sheets Hall effects may play a role for the precise structure of these sheets because the magnetic field would be frozen to the electron fluid rather than the bulk motion. However, these are interesting topics for future work and require the background of the presented MHD results.

Acknowledgments. The work is supported by the NASA SR&T grant NAG 5-6219 to the University of Alaska Fairbanks. The computation is supported by Arctic Region Supercomputer Center at the University of Alaska Fairbanks.

References

- Axford, W. I., and C. O. Hines, A unifying theory of high latitude geophysical phenomena and geomagnetic storms, *Can. J. Phys.*, **39**, 1433, 1961.
- Birn, J., Computer studies of the dynamical evolution of the geomagnetic tail, *J. Geophys. Res.*, **85**, 1214, 1980.
- Birk, G.T., H. Wiechen, and A. Otto, Magnetic field amplification in M82 winds caused by Kelvin-Helmholtz modes, submitted *Ap.J.*, 1999.
- Borovsky, J. E., M.F. Thomsen, R. C. Elphic, The driving of the plasma sheet by the solar wind, *J. Geophys. Res.*, **103**, 17,617, 1998.
- Chandrasekhar, S., *Hydrodynamic and Hydromagnetic Stability*, Oxford University Press, New York, 1961.
- Chen, Q., A. Otto, and L.C. Lee, Tearing instability, Kelvin-Helmholtz instability, and magnetic reconnection, *J. Geophys. Res.*, **102**, 151, 1997.
- Chen, S.H. and M.G. Kivelson, On non-sinusoidal waves at the Earth's magnetopause, *Geophys. Res. Lett.*, **20**, 2699, 1993.
- Chen, S.H., M.G. Kivelson, J.T. Gosling, R.J. Walker, and A.J. Lazarus, Anomalous aspects of magnetosheath flow and of the shape and oscillations of the magnetopause during an interval of strongly northward interplanetary magnetic field, *J. Geophys. Res.*, **98**, 5727, 1993.
- Dungey, J. W., Interplanetary magnetic field and the auroral zones, *Phys. Rev. Lett.*, **6**, 47, 1961.
- Fairfield, D.H., et al., Geotail observations of an unusual magnetotail under very northward IMF conditions, *J. Geomag. and Geoelectr.*, Vol. 48, 473, 1996.
- Fairfield, D.H., R.P. Lepping, A. Otto, T. Mukai, T. Yamamoto, S. Kokubun, J.T. Steinberg, A.J. Lazarus, Kelvin-Helmholtz instability at the magnetotail boundary: MHD simulation and comparison with Geotail observations, submitted *J. Geophys. Res.*, July, 1999.
- Fujimoto, M., and T. Terasawa, Anomalous ion mixing within an MHD scale Kelvin-Helmholtz vortex, *J. Geophys. Res.*, **99**, 8601, 1994.
- Fujimoto, M., and T. Terasawa, Anomalous ion mixing within an MHD scale Kelvin-Helmholtz vortex, 2, Effects of inhomogeneity, *J. Geophys. Res.*, **100**, 12,025, 1995.
- Fujimoto, M., A. Nishida, T. Mukai, Y. Saito, T. Yamamoto, and S. Kokubun, Plasma Entry from the flanks of the near-Earth magnetotail: Geotail observations in the dawnside LLBL and the plasma sheet, *J. Geomag. and Geoelectr.*, Vol. 48, 711, 1996.
- Fujimoto, M., T.M.H. Kawano, M. Nakamura, A. Nishida, Y. Saito, T. Yamamoto, and S. Kokubun, Structure of the low-latitude boundary layer: A case study with Geotail data, *J. Geophys. Res.*, **103**, 2297, 1998a.
- Fujimoto, M., T. Terasawa, T. Mukai, Y. Saito, T. Yamamoto, and S. Kokubun, Plasma Entry from the flanks of the near-Earth magnetotail: Geotail observations, *J. Geophys. Res.*, **103**, 4391, 1998b.
- LaBelle-Hamer, A.L., A. Otto, and L.C. Lee, Magnetic reconnection in the presence of sheared flow and density asymmetry: Applications to the Earth's magnetopause, *J. Geophys. Res.*, **100**, 11875, 1995.
- Lee, L. C., and Z. F. Fu, A theory of magnetic flux transfer at the Earth's magnetopause, *Geophys. Res. Lett.*, **12**, 105, 1985.
- Liu, Z.X., and Y.D. Hu, Local magnetic field reconnection caused by vortices in the flow field, *Geophys. Res. Lett.*, **15**, 752, 1988.
- Miura, A., and P. L. Pritchett, Nonlocal Stability Analysis of the MHD Kelvin-Helmholtz Instability in a Compressible Plasma, *J. Geophys. Res.*, **87**, 7431, 1982.
- Miura, A., Anomalous Transport by magnetohydrodynamic Kelvin-Helmholtz instabilities in the solar wind magnetosphere interaction, *J. Geophys. Res.*, **89**, 801, 1984.
- Miura, A., Kelvin-Helmholtz Instability at the magnetospheric boundary: dependence on the magnetosheath sonic Mach number, *J. Geophys. Res.*, **97**, 10,655, 1992.
- Miura, A., Self-organization of the two-dimensional magnetohydrodynamic transverse Kelvin-Helmholtz instability, *J. Geophys. Res.*, **104**, 395, 1999a.
- Miura, A., A quantitative test of the self-organization hypothesis of the magnetopause Kelvin-Helmholtz instability as an inverse problem, *Geophys. Res. Lett.*, **26**, 409, 1999b.
- Otto, A., and G. T. Birk, Resistive Instability of Periodic Current Sheet, *Phys. Fluids, B* **4**(11), 3811, 1992.
- Otto, A., 3-D resistive MHD computations of magnetospheric physics, *Comput. Phys. Commun.*, **59**, 185, 1990.

- Otto A., L.C. Lee, and Z.W. Ma, Plasma and magnetic field properties associated with pressure pulses and magnetic reconnection at the dayside magnetopause, *J. Geophys. Res.*, 14895, 1995.
- Petschek, H. G. Magnetic Annihilation, in *AAS-NASA Symposium on the Physics of Solar Flares*, ed. by W. N. Hess, p. 425, NASA Spec. Publ. SP-50, 1964.
- Potter, D.E., *Computational Physics*, John Wiley, New York, 1973.
- Pu, Z. Y., M. Yan, and Z. X. Liu, Generation of Vortex Induced-tearing Mode Instability at the Magnetopause, *J. Geophys. Res.*, 95, 10,559, 1990.
- Scholer, M., Magnetic flux transfer at the magnetopause based on single X line bursty reconnection, *Geophys. Res. Lett.*, 15, 291, 1988.
- Sonnerup, B.U.Ö., I. Papamastorakis, G. Paschmann, and H. Luhr, The magnetopause for large magnetic shear: Analysis of convection electric fields from AMPTE/IRM, *J. Geophys. Res.*, 95, 10541, 1990.
- Terasawa, T., Hall Current Effect of Tearing Mode Instability, *Geophys. Res. Lett.*, 10, 6, 475, 1983.
- Thomas, V. A., and D. Winske, Kinetic simulations of the Kelvin-Helmholtz instability at the magnetopause, *J. Geophys. Res.*, 98, 11,425, 1993.
- Wei, C. Q., and L. C. Lee, Coupling of magnetopause-boundary layer to the polar ionosphere, *J. Geophys. Res.*, 98, 5707, 1993.
- Wu, C. C., Kelvin-Helmholtz Instability at the Magnetopause Boundary, *J. Geophys. Res.*, 91, 3042, 1986.
- Yan M., A. Otto, D. Muzzel, and L.C. Lee, Tearing mode instability in a multiple current sheet system, *J. Geophys. Res.*, 99, 8657, 1994.

A. Otto, Geophysical Institute, University of Alaska, Fairbanks, AK 99775-7320. (ao@why.gi.alaska.edu)

Received _____

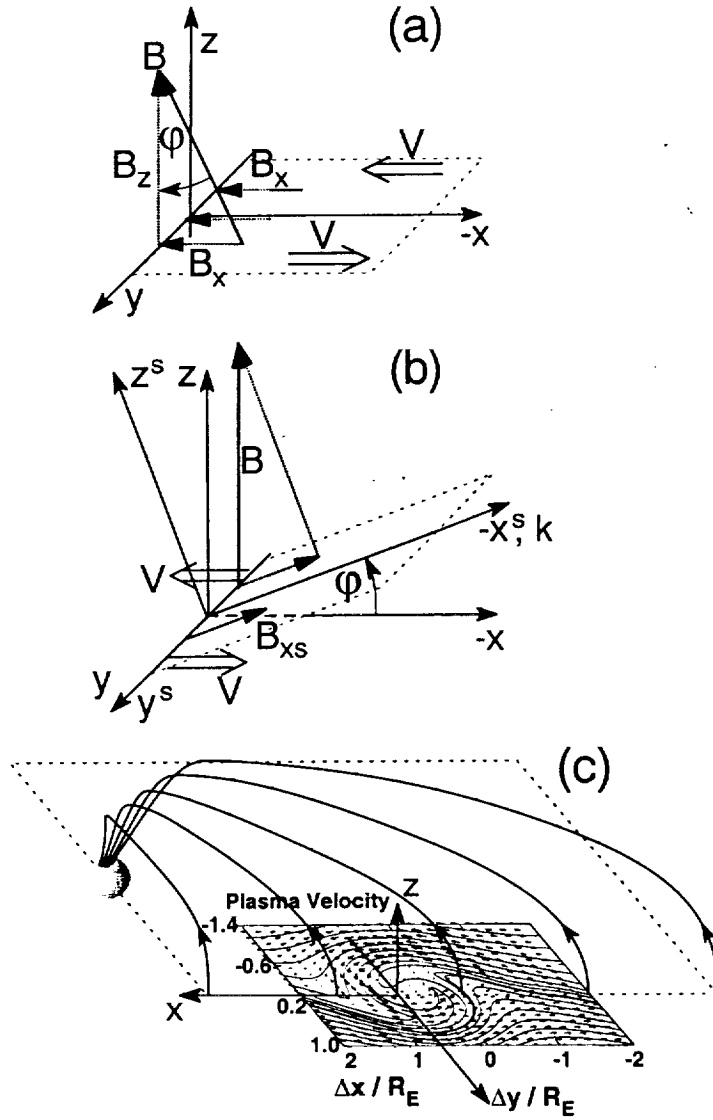


Figure 1. Illustration of basic geometries for the occurrence of KH instabilities on the magnetospheric flank: (a) The k vector of the KH mode is in the equatorial plane and the magnetospheric and the magnetosheath fields have a small x component; (b) the magnetospheric and magnetosheath fields are along the z direction and the k vector has a component out of the equatorial plane (the upper index s denotes simulation coordinates); (c) illustration of the KH mode at the magnetospheric boundary. In the cases (a) and (b) the angle between the k vector and the magnetic field is $90^\circ - \phi$.

Magnetic Field and Plasma Velocity

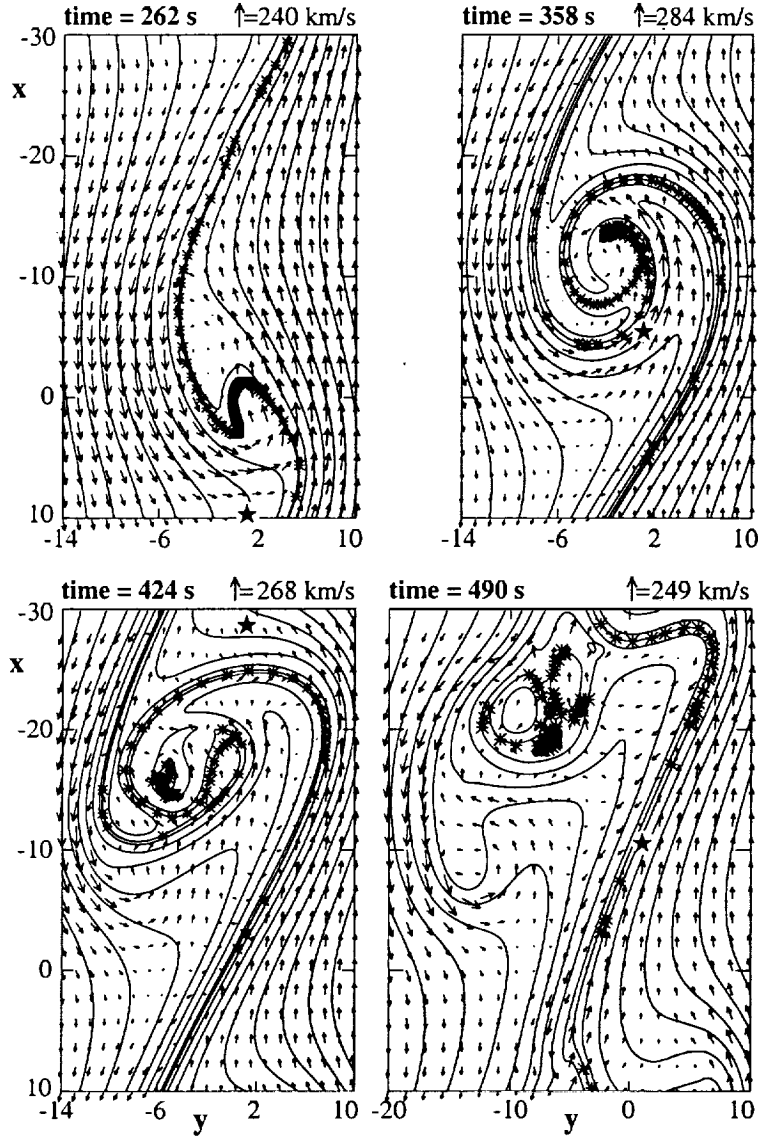


Figure 2. Plots of magnetic field lines (projected into the simulation plane) and velocity vectors to illustrate the evolution of the KH mode for the reference case. The four plots correspond to four times and the asterisks indicate the location of the initial boundary. The star in each plot shows the instantaneous location at which data are recorded for Figure 5.

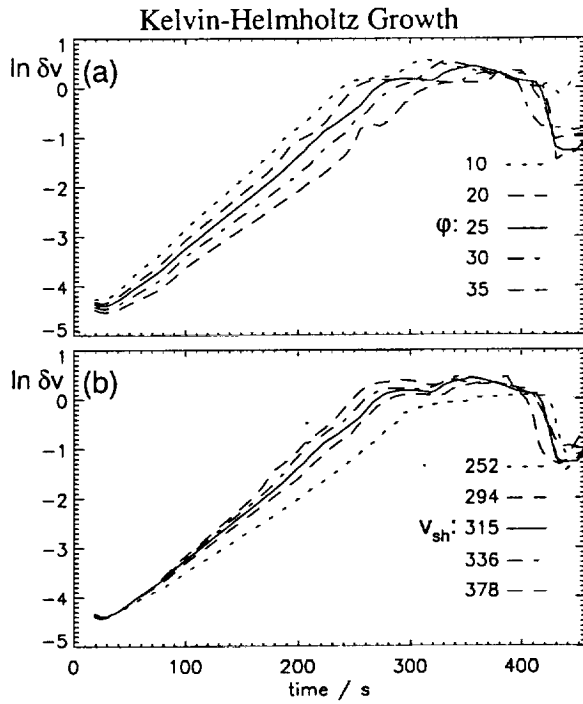


Figure 3. Plot of $\ln \delta v$ as a function of time to measure the growth of the KH mode as a function the angle φ (measured in degrees) in the plot (a)) and as a function of magnetosheath velocity (in km s^{-1}) in the plot (b).

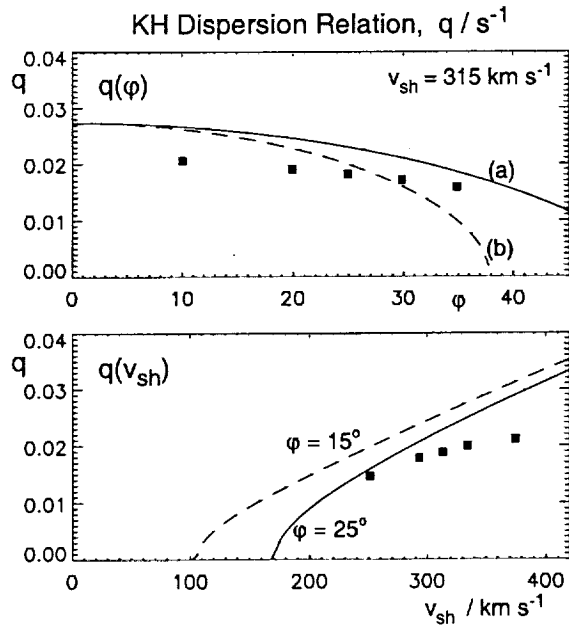


Figure 4. Plots of the KH growth rate obtained from the dispersion relation as a function of the angle φ (upper plot) and of the magnetosheath velocity (bottom plot). The line (a) in the upper plot shows the growth rate for the configuration sketched in Figure 1a and the line (b) corresponds to the configuration of Figure 1b. The black squares indicate the corresponding growth rates from the simulation results in Figure 3

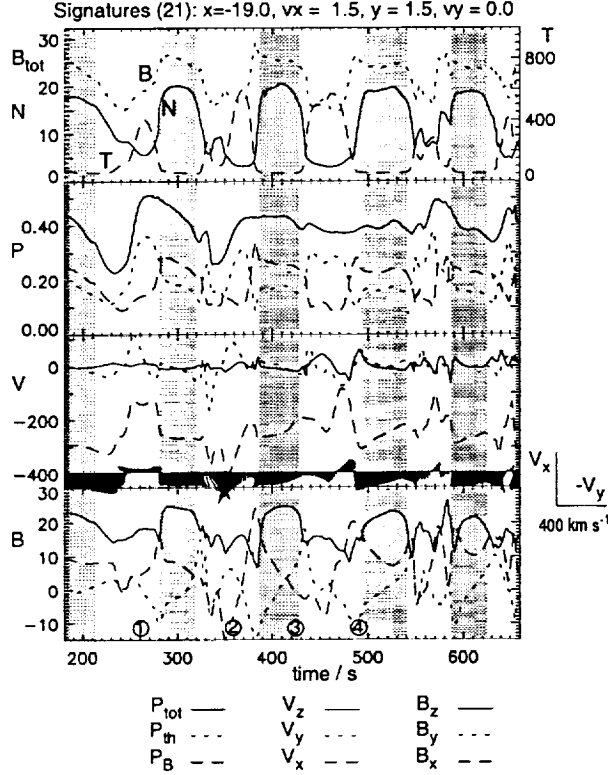


Figure 5. Signatures recorded for the reference case of the total magnetic field B_{tot} (in nT), number density (in cm^{-3}), temperature (in eV) in the uppermost panel; thermal, magnetic, and total static pressure (in nPa) in the second panel; plasma velocity components (in km s^{-1}) in the third panel; and magnetic field components (in nT) in the bottom panel. Shaded are regions of high magnetosheath-like number density. The vectors in the velocity panel show the direction of the velocity with an average of -180 km s^{-1} subtracted. The data are recorded at the location $y = 1.5$ corresponding to 900 km outside the initial boundary.

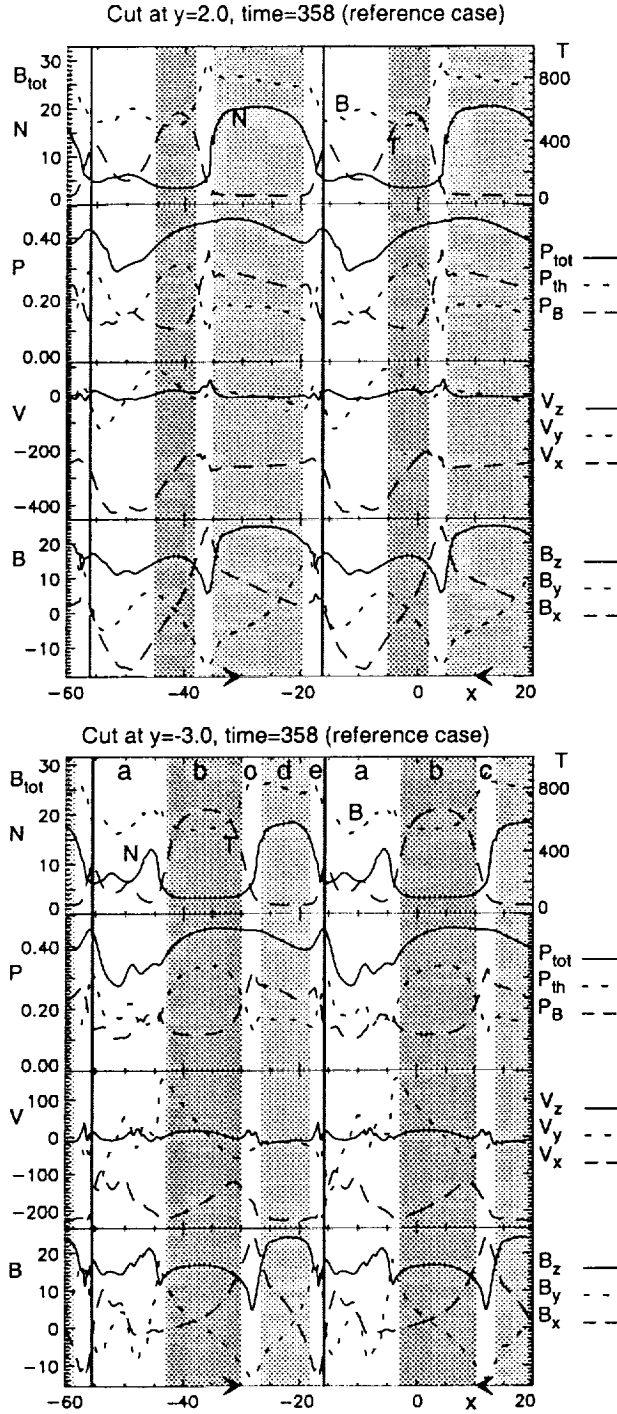


Figure 6. Plasma properties as in Figure 5 now obtained by a cut through the two dimensional system at $y = 2$ (1200 km) and at $y = -3$ (-1800 km) at the time 358 s for the reference case. Light shading denotes regions of high density, dark shading denotes regions of high temperature, and the thin vertical line denotes an additional boundary (see text).

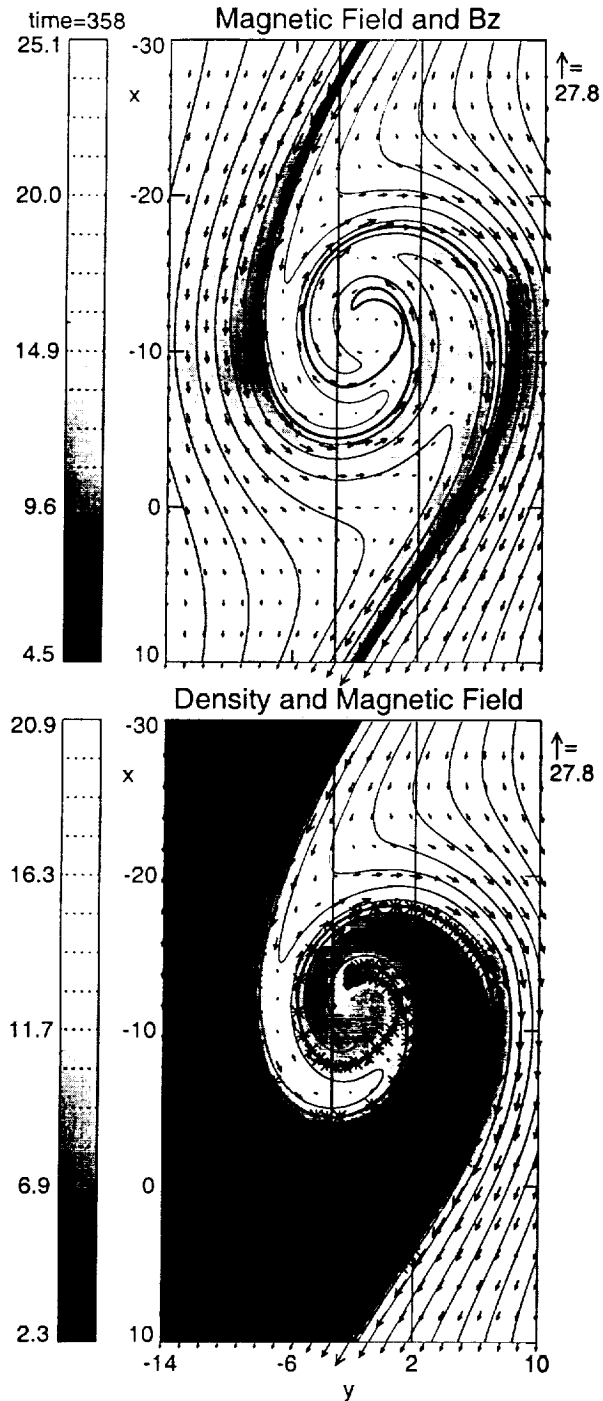


Figure 7. The upper plot shows magnetic field lines (projected into the simulation plane), magnetic field vectors (in the simulation plane), and the B_z component in gray scale. The vertical lines indicate the location for the cuts shown in Figure 6. The lower plot shows the number density as a gray scale plot in addition to field lines and vectors. Magnetic field and number density are measured in nT and particles per cm³.

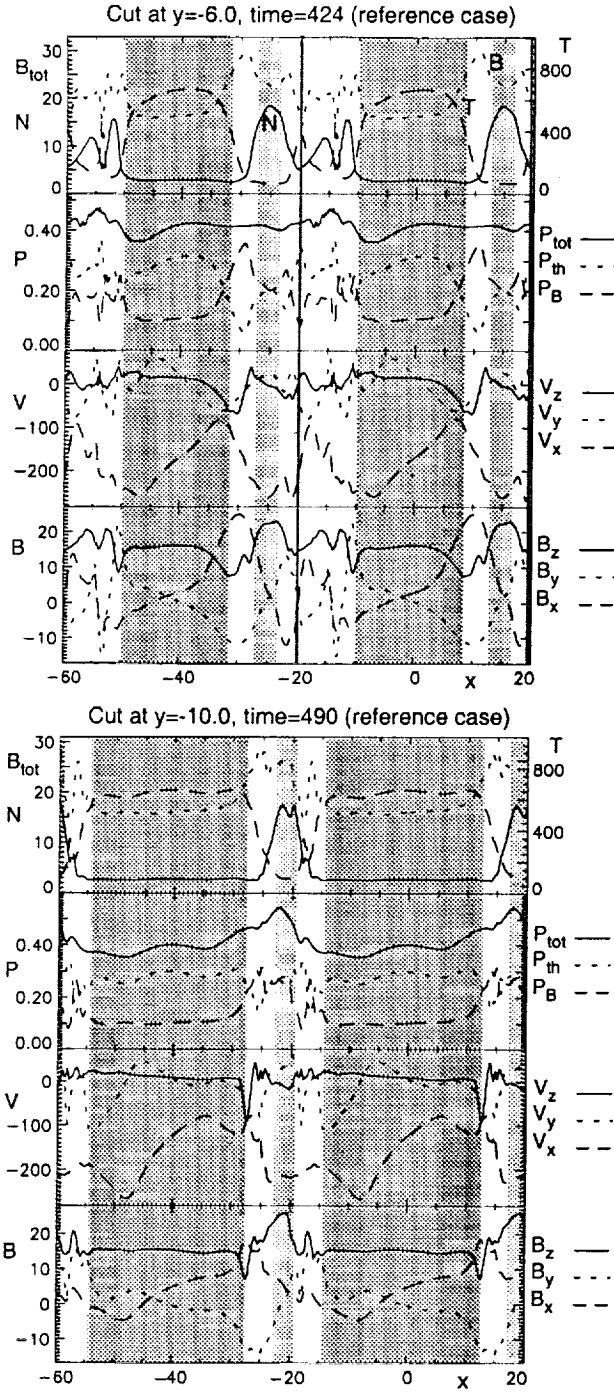


Figure 8. Plasma and magnetic field properties in a cut at $y = -6$ (-3600 km) for the time 424 s (upper plot) and at $y = -10$ (-6000 km) for the time 490 s (bottom plot). Both plots are for the reference case in the same format as Figure 6.

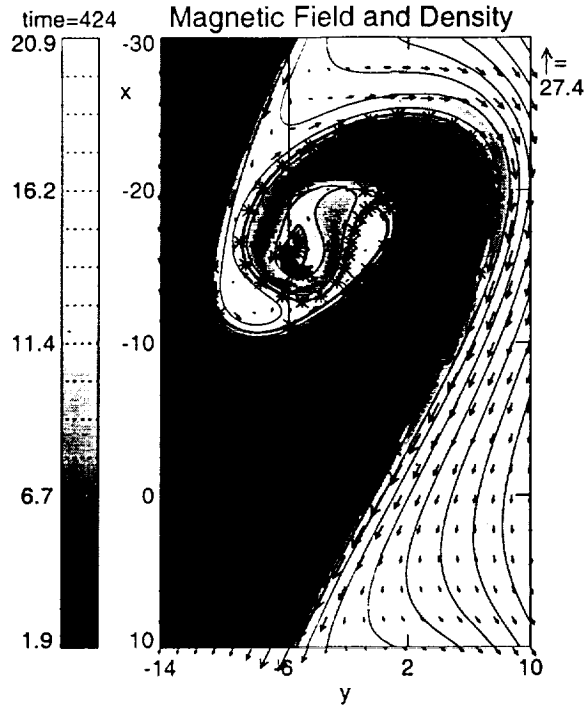


Figure 9. Magnetic field lines and field vectors projected into the simulation plane overlaid on a gray scale plot of the plasma number density at the time 424 s coincident with the upper plot in Figure 8. The asterisks indicate plasma elements from the original boundary. Units are in nT and cm^{-3} .

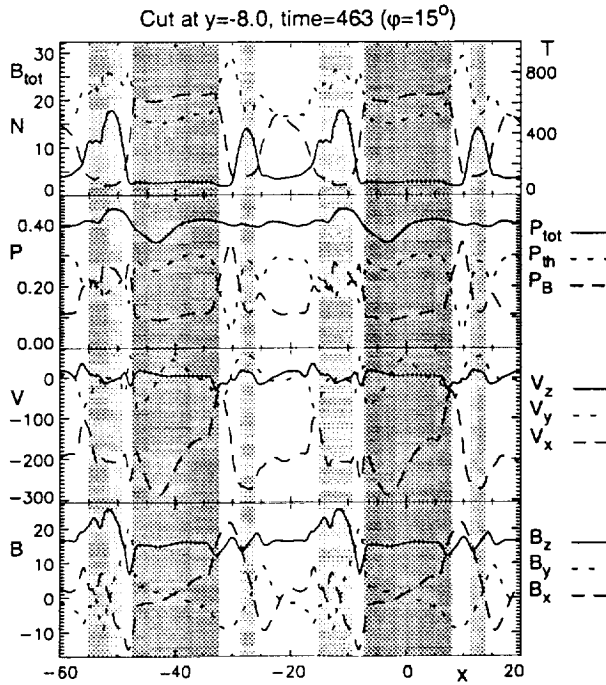


Figure 10. Plasma and magnetic field properties in a cut at $y = -8$ (-4800 km) for the time 463 s for the case with $\varphi = 15^\circ$. Both The plots use the same format as Figure 6.

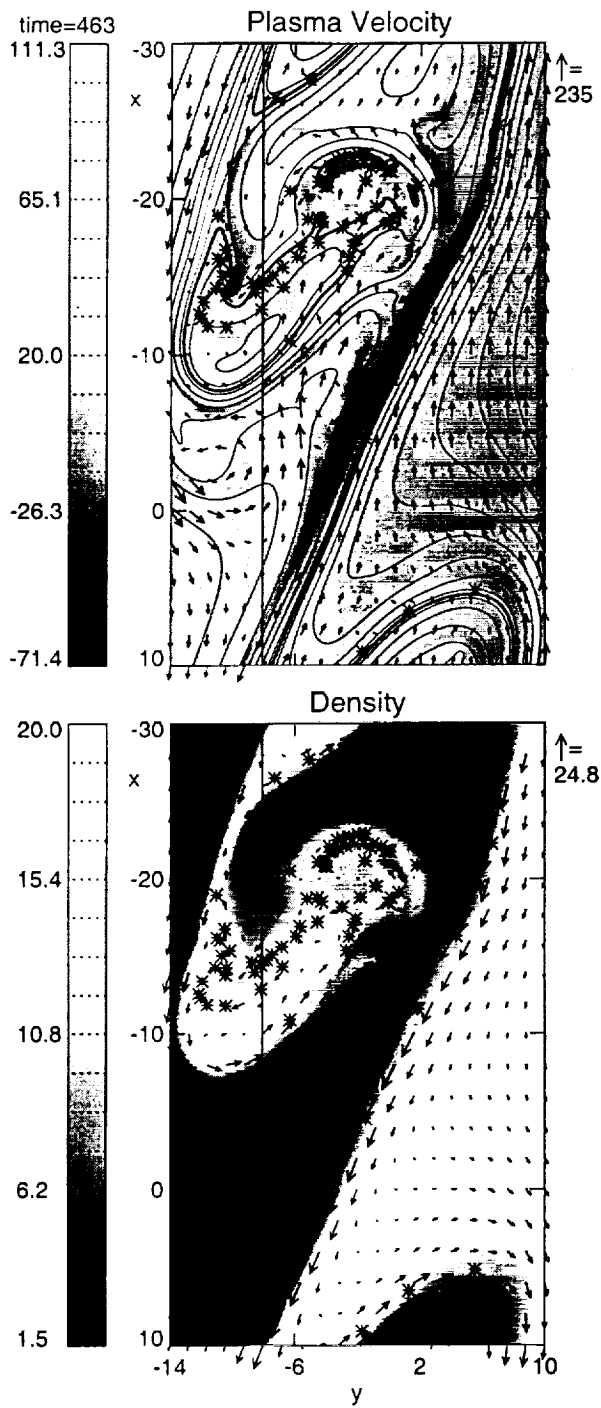


Figure 11. Plasma velocity (x and y components as vectors and the z component as a gray scale) and magnetic field lines in the upper plot for the time 463 s and the case with $\varphi = 15^\circ$. The bottom plot represents density combined with magnetic field vectors. The asterisks indicate plasma elements from the initial boundary.

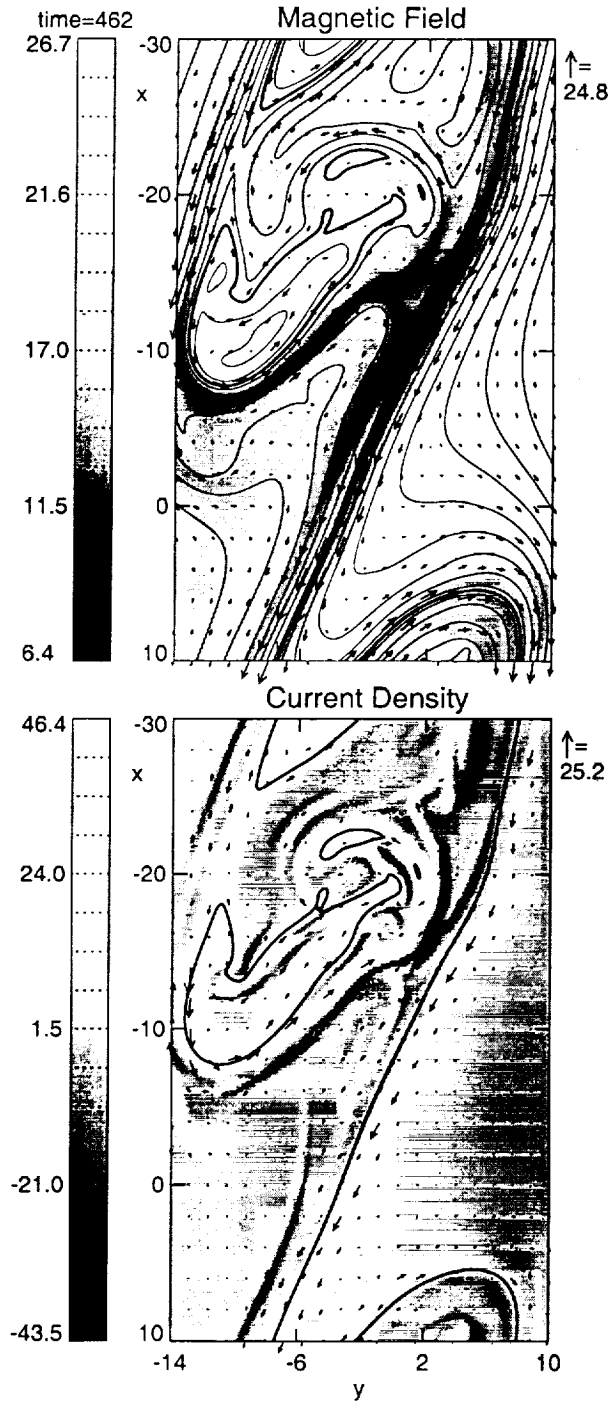


Figure 12. Magnetic field lines and vectors projected into the simulation plane and a gray scale plot of the B_z component for $\varphi = 15^\circ$ at time 462 s in the upper figure. The bottom plot shows current density vectors j_x , and j_y in the simulation plane and a gray scale representation of j_z for $\varphi = 15^\circ$. The line in the bottom figure is chosen to represent the initial boundary.

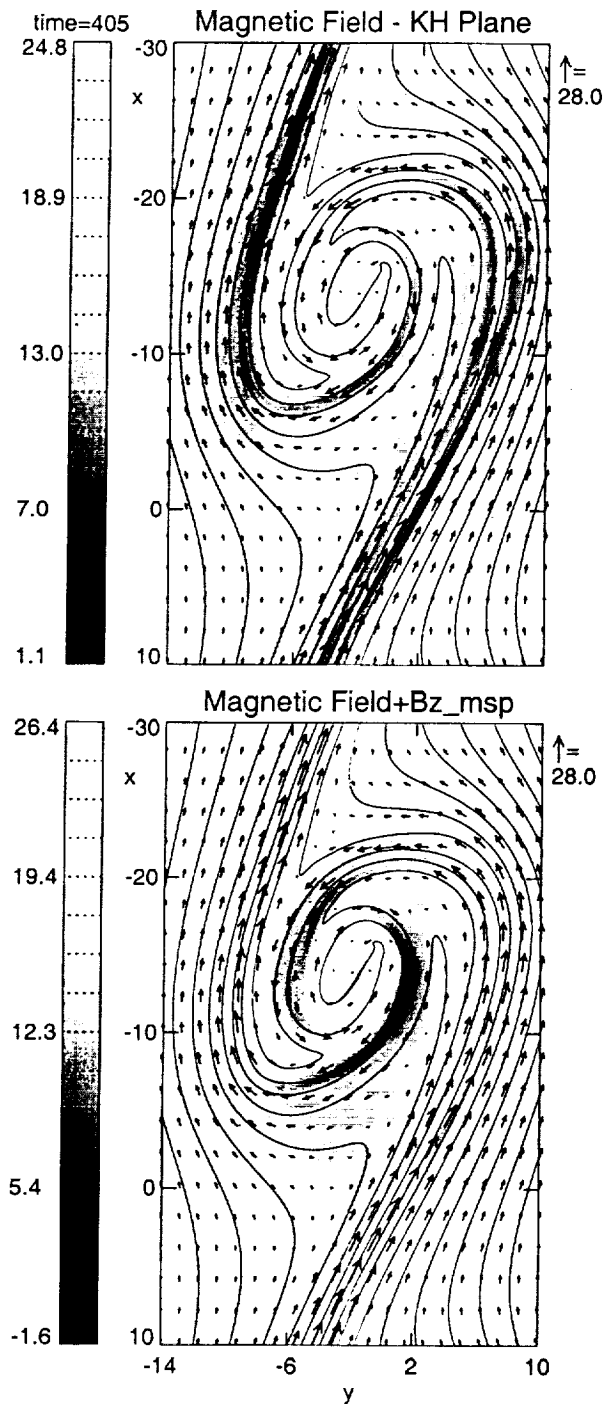


Figure 13. Magnetic field lines and vectors for the case representing the configuration from Figure 1b. In gray scale the upper plot presents the B_z component from the simulation geometry, while the lower plot shows the B_z component projected back into the 'magnetospheric' coordinate system.

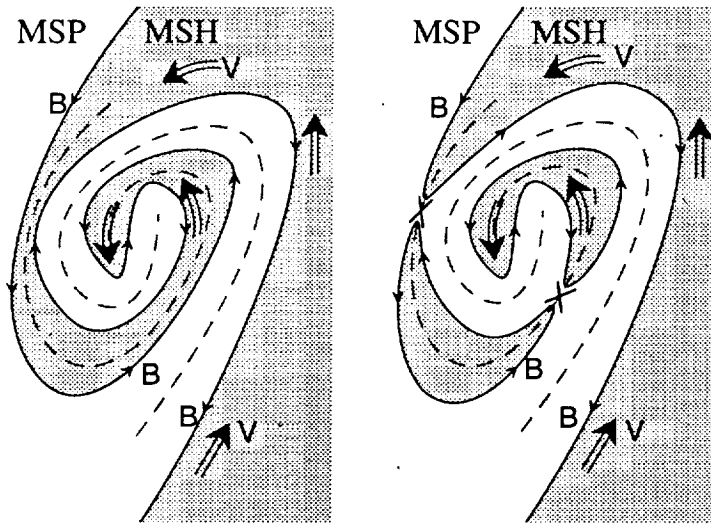


Figure 14. Sketch of the evolution of magnetic reconnection in the Kelvin-Helmholtz vortex.

Table 1. Normalization Units

Quantity	Units
Magnetic Field B_0	16 nT
Number Density n_0	11 cm ⁻³
Current Density	22 nA m ⁻²
Length Scale L_0	600 km
Velocity v_A	105 km s ⁻¹
Time τ_A	5.7 s

Table 2. Initial Plasma Parameters

Location	B	V	ρ	β
M'sphere	16 nT	0 km s ⁻¹	2.8 cm ⁻³	2.8
M'sheath	24 nT	315 km s ⁻¹	19.2 cm ⁻³	0.69

Table 3. Initial Plasma Parameters

Case	V	φ	Config
1	252 km s ⁻¹	25	(a)
2	294 km s ⁻¹	25	(a)
3	315 km s ⁻¹	25	(a)
4	336 km s ⁻¹	25	(a)
5	378 km s ⁻¹	25	(a)
6	315 km s ⁻¹	10	(a)
7	315 km s ⁻¹	15	(a)
8	315 km s ⁻¹	20	(a)
9	315 km s ⁻¹	30	(a)
10	315 km s ⁻¹	35	(a)
11	315 km s ⁻¹	25	(b)